Coupling light to periodic nanostructures

Driessen, E.F.C.

Chapter 2

Fano resonances and waveguide modes in a two-dimensional photonic-crystal slab

The measured reflection spectra of two-dimensional photonic crystal slabs consist of an asymmetric peak on top of an oscillating background. For p-polarized light, this asymmetric peak changes shape, when the angle of incidence is tuned over Brewster's angle. We explain the observed line shapes with a Fano model that includes loss and use a waveguide model to predict the resonance frequencies of the photonic-crystal slab. Finite-difference time domain calculations support the model and show that resonances due to higher order waveguide modes disappear when the substrate refractive index is increased beyond $n_{\mathrm{s}} = 2.04$. This is readily explained by the cut-off condition of these modes, given by the waveguide model.

This chapter is based on E. F. C. Driessen, P. O. M. Heemskerk, D. Stolwijk, E. W. J. M. van der Drift, and M. J. A. de Dood, *Asymmetry reversal and waveguide modes in the reflection from a two-dimensional photonic-crystal slab*, Proc. SPIE **6989**, 69890G (2008).

2.1 Introduction

Resonant optical structures, in particular photonic crystals embedded in a waveguide, form an important class of optical materials. These photonic-crystal slabs contain a periodic arrangement of holes on a wavelength scale, and allow control of the propagation of light, guided in the plane of the waveguide [16]. For example, they enable wavelength-dependent steering [17], strong coupling of atoms to a cavity [18], and enhanced non-linear optical effects [8].

A measurement of the reflectivity as a function of the wavelength is a relatively easy way to characterize the optical properties of these slabs. At each angle of incidence, the reflectivity spectrum shows a number of resonant features related to coupling of incident radiation to a leaky waveguide mode of the photonic-crystal slab [19, 20]. The reflection spectra can be calculated numerically by solving Maxwell's equations using a scattering-matrix approach [21, 22], Green's functions [23], or finite-difference time domain (FDTD) methods [19, 24]. Although these numerical solutions of Maxwell's equations predict the right frequencies and quality factors of the resonances observed in the measurements, they do not give physical insight into the origin of the spectral features. Therefore, it is important to develop simpler models to explain the measured resonances. Such models can be used as a diagnostic tool for fabricated structures, and can facilitate the first design of a photonic crystal structure.

Here, we present reflection measurements on a two-dimensional (2-D) photonic-crystal slab. We use an extended coupled-mode theory to describe the shape of the measured reflectivity spectra and the line shape of the resonant features. This theory explains the change in asymmetry that is observed when changing the angle of incidence, as resulting from the change of sign of the Fresnel reflection coefficient of the layered structure at Brewster's angle. We use a waveguide model [25, 26] to predict the resonance frequencies of a photonic-crystal slab and compare this model to FDTD calculations. The disappearance of modes from the spectra when increasing the refractive index of the substrate is explained by the model in terms of the cut-off condition of the guided modes.

2.2 Photonic crystal fabrication

The GaAs and AlGaAs photonic crystals in this study were fabricated using a combination of electron-beam lithography and reactive ion etching*. A square lattice of 1000×1000 holes, with a radius $r \approx 100$ nm and a lattice constant $a \approx$

*The detailed fabrication recipe can be found in Appendix A

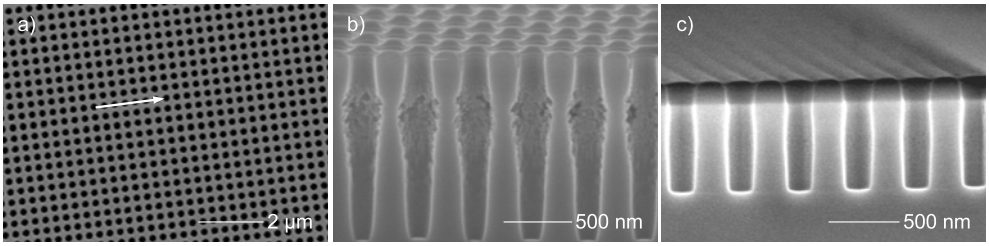

Figure 2.1. SEM images of photonic crystal structures fabricated by reactive ion etching in a Cl_2/N_2 plasma. (a) Top view of the photonic crystal structure used for the measurements in Sec. 2.4. The arrow corresponds to the direction of $k_{\|}$ in the reflection measurements. (b) Cross section (taken under an angle of 45°) of the etched holes when no N_2 is added. The non-passivated side walls are partially etched away by the plasma. (c) Cross section of the holes (taken under an angle of 55°) when 10 sccm of N_2 is added to passivate the side walls. The silicon nitride mask on top is still visible.

320 nm, was defined by electron-beam lithography in a $\sim$ 550 nm thick layer of ZEP 520 positive-tone resist* on top of a $\sim$ 300 nm layer of silicon nitride. After development, the pattern was transferred to the nitride by reactive ion etching using a low pressure (< 8 μbar) CHF_3:Ar (1:1) plasma. The remaining ZEP resist was removed with an oxygen plasma.

The resulting hole pattern in the nitride serves as a mask for reactive ion etching of the (Al)GaAs with a chlorine-based plasma [5, 27]. In this process, the chlorine ions etch the (Al)GaAs, while the nitrogen is used to passivate the side walls. We used a power of 100 W, a pressure < 5 μbar, and a flow of 15 sccm BCl_3 and 7.5 sccm Cl_2, and varied the N_2 flow to tune the profile of the side walls. The selectivity of the etching process is $> 10:1$, and the etch rate depends on the hole size and the nitrogen flow, i.e. $\sim$ 200 nm/min for holes with a diameter of 300 nm, and $\sim$ 1 μm/min for holes with a diameter of 1 μm, with N_2 added. Figure 2.1(a) shows a scanning electron microscope (SEM) image of the photonic crystal after the fabrication process. Figure 2.1(b) shows a cross section of the holes when using a plasma without N_2 added, showing damage to the side walls of the holes. In Fig. 2.1(c), we added a flow of 10 sccm N_2 to the plasma, resulting in straight holes. A slight curvature of the holes is observed in Fig. 2.1(c). The curvature is due to specular reflection of the ions from the slightly tapered nitride mask, and the depth at which it occurs depends on the hole diameter. This curvature is therefore not intrinsic to the

*ZEON corporation, http://www.zeon.co.jp

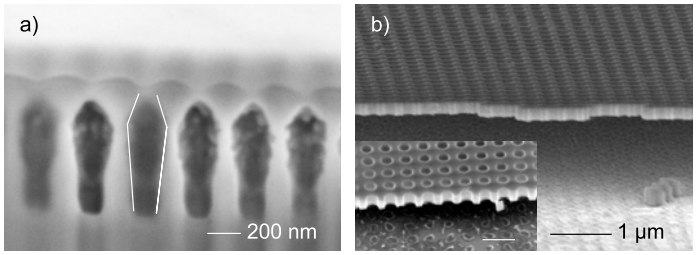

Figure 2.2. SEM images of (a) the cross section of the photonic crystal used for the measurements in section 2.4 (taken under an angle of 59°). The approximate shape of the holes is indicated with the white curves. (b) A large, high-quality, free-standing photonic-crystal membrane. The GaAs capping layer is not removed from the membranes in this picture. The inset shows an enlarged image of the holes. The length of the scale bar in the inset is 500 nm.

process and straight holes as deep as a few microns can easily be achieved. In the final stage, we selectively removed the silicon nitride mask using the same CHF_3:Ar reactive ion etch used to define the mask.

Figure 2.2 shows SEM images of photonic crystal samples that consist of a higher refractive index slab layer on top of a substrate with a lower index. The structure in Fig. 2.2(a) was fabricated in a GaAs substrate using a relatively low N_2 flow, leading to incomplete passivation of the side walls. The lines in the figure indicate the resulting tapering of the holes. The undercut effectively defines a waveguide structure that was used in the optical measurements of Sec. 2.4.

The same reactive ion etch can be used to define high quality photonic crystals in a free-standing membrane. Figure 2.2(b) shows a part of such a membrane structure, consisting of 1000×1000 holes ($\sim 300\times300\ \mu m^2$). To fabricate this structure, we used a GaAs substrate with a heterostructure consisting of a 1000 nm $Al_{0.7}Ga_{0.3}As$ sacrificial layer, a 300 nm thick $Al_{0.35}Ga_{0.65}As$ membrane layer, and a 100 nm thick GaAs capping layer to prevent oxidation. After transferring the photonic crystal pattern to the heterostructure, we selectively removed the GaAs capping layer, using a wet etch of peroxide and citric acid [28]. In the last step, a wet etch with hydrofluoric acid was used to selectively remove the aluminium-rich sacrificial layer [5], thus creating the free-standing photonic-crystal membrane in Fig. 2.2(b). Note that the curvature of the holes due to the tapered nitride mask occurs in the sacrificial layer in this case.

2.3 Theory

The reflection spectrum of a photonic-crystal slab typically consists of an oscillating background and a number of sharp resonances [19, 20] as shown in Fig. 2.4 and Fig. 2.6. The spectrum can be explained using a simple scattering model of a resonator coupled to a continuum of modes. The photonic-crystal slab, that acts as the resonator, is depicted in Fig. 2.3(a), together with the input and output ports. Part of the radiation incident on the slab is diffracted into a leaky waveguide mode (dashed arrows), whereas another part is directly reflected and transmitted (solid arrows). The radiation that is diffracted back from the waveguide mode interferes with the directly reflected and transmitted radiation, yielding the characteristic Fano line shape [29]. In Sec. 2.3.1 we extend a temporal coupled-mode theory [30] to include loss, and describe the reflection in terms of the parameters of the direct and resonant channels. After that, in Sec. 2.3.2, we introduce a waveguide model to predict the resonance frequency of the resonant channel.

2.3.1 Fano model

To calculate the spectrum of the transmitted and reflected light, we proceed as follows. For each angle of incidence and each wavelength, a scattering matrix links the amplitudes of the incident, reflected, and transmitted waves. The scattering matrix S of the system is the sum of the scattering matrices of the direct and the resonant channel. The direct channel is described by a scattering matrix C, given by

$$C = \begin{pmatrix} r_1 & t_{21} & \cdots \\ t_{12} & r_2 & \\ \vdots & & \ddots \end{pmatrix}, \tag{2.1}$$

that connects the amplitudes of the modes (ports) on both sides of the slab. When there are no propagating diffraction orders in the media above and below the guiding layer, the components of the scattering matrix are given by the Fresnel reflection and transmission coefficients for a homogeneous layered system. The contribution from the direct channel gives rise to typical oscillations in the reflectivity as a function of wavelength (Fabry-Perot fringes). If there are propagating diffraction orders in the media above or below the guiding layer, a more elaborate method is needed to calculate the matrix elements of C.

The resonant channel corresponds to a coupling of the incident radiation to a single leaky waveguide mode via diffraction from the periodic photonic

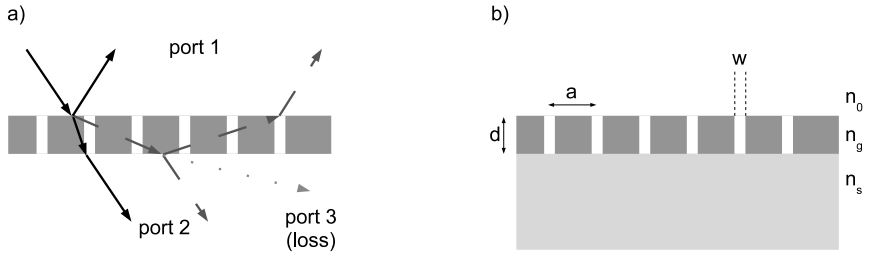

Figure 2.3. (a) Schematic drawing of the direct and resonant reflection and transmission in a photonic-crystal slab. The incident light in port 1 can be scattered via the direct channel (solid arrows) or diffracted into a waveguide mode (resonant channel, dashed line). The waveguide losses can be modeled by including a third port (dotted arrow) to the system. (b) Geometry of the photonic-crystal slab used in the FDTD calculations in section 2.3.2. The slab of thickness d and refractive index n_{g} contains a periodic array of air slits with a width w and a periodicity a. The slab is supported by a substrate with refractive index n_{s}, and covered by air ($n_0 = 1$) on the top.

crystal structure. For a fixed angle of incidence, the coupling to a specific waveguide mode p occurs at a resonance frequency ω_p and is characterized by an escape rate γ_p. This escape rate parametrizes the life time of light in the waveguide mode. The coupling to the waveguide mode is described by coupling constants $d_{j,p}$, where the index j corresponds to the different ports coupling to the waveguide mode. The coefficients γ_p, $d_{j,p}$, and the matrix elements C_{jk} are not independent. Time-reversal symmetry and energy conservation put the following constraints on the coupling constants (a derivation of these conditions is given in Ref. 30):

$$\sum_j |d_{j,p}|^2 = 2\gamma_p, \tag{2.2}$$

$$\sum_k C_{jk} d^*_{k,p} = -d_{j,p}, \tag{2.3}$$

where the indices j and k refer to the different ports, and C_{jk} are the elements of the direct transmission matrix connecting the different free-space modes. Equation (2.3) links the amplitude and phase of the coupling constants to the scattering matrix C of the direct process.

The matrix elements of the scattering matrix S for the combined system

of direct and indirect coupling are given by

$$S_{jk} = C_{jk} + \sum_p \frac{d_{j,p} d_{k,p}}{i(\omega - \omega_p) + \gamma_p}, \tag{2.4}$$

where ω is the angular frequency of the incident radiation. The reflection coefficients for the different ports are given by the diagonal elements of this matrix, and the transmission coefficients by the off-diagonal elements. This description which uses a Lorentzian line shape for the resonant channel, is a simplification which holds as long as $\omega_p \ll \Gamma_p + \gamma_p$. The small frequency shift that results from describing our resonance with a Lorentzian can be included in the resonance frequencies ω_p. It is important to stress that the equations derived here hold for the case of *uncoupled* waveguide modes only. For the modes to be uncoupled, it is necessary that the number of independent ports, i.e. the rank of the matrix C_{ij}, is larger than or equal to the number of waveguide modes p [31].

Losses can be included in the description in this model, by discriminating between losses in the direct channel, due to absorption or surface roughness, and losses in the resonant channel. Losses in the resonant channel can also be due to scattering of the waveguide mode to ports that are not incorporated in the scattering matrix description.

Absorption losses in the direct scattering channel can be adequately described by using a non-unitary scattering matrix C and the Fresnel coefficients of a layered system with complex-valued refractive index. This matrix can be made unitary by adding an extra port to the description. If we assume that the input in this extra port is zero, and that the loss port is not coupled to the resonator mode, then the scattering matrix S includes a block matrix describing the normal input and output ports of the system, that is not influenced by the parameters of the loss port. This makes it possible to use Eqs. (2.2)-(2.4), while using a non-unitary scattering matrix C for the direct channel.

Waveguide losses can be incorporated in a similar way, by extending the model with extra loss ports, which only couple to the specific waveguide modes. Each waveguide mode couples to its loss port with a coupling constant Γ_p. The direct scattering matrix for a two-port system with an additional loss port acquires the form

$$C = \begin{pmatrix} r_1 & t_{21} & 0 \\ t_{12} & r_2 & 0 \\ 0 & 0 & 1 \end{pmatrix}. \tag{2.5}$$

The loss rates Γ_p are incorporated in Eq. (2.2) in a straightforward way, by using the convention $\sum_j |d_{j,p}|^2 = 2\,(\gamma_p + \Gamma_p)$, where the index j now runs over

all ports.

For the symmetric case of two ports coupled to only one leaky waveguide mode, symmetry requires that $r_1 = r_2 = r$ and $t_{21} = t_{12} = it$, where r and t are real. Moreover, the coupling constants to the ports should be equal, except for a plus or minus sign determined by the odd or even symmetry of the waveguide mode with respect to the mirror plane. The reflectivity in this case is given by

$$R = \left| r + \gamma \frac{-r \mp it}{i(\omega - \omega_0) + \gamma + \Gamma} \right|^2, \tag{2.6}$$

where the $\mp$ is determined by the even or odd symmetry of the mode [30], and the parameters ω, γ, and Γ lost their subscripts since we are dealing with only one waveguide mode. This expression gives the typical asymmetric Fano line shape. The reflectivity has a distinct zero if the loss rate $\Gamma = 0$. To reach 100% reflectivity, the direct process has to be lossless as well (i.e. $|r|^2 + |t|^2 = 1$).

2.3.2 Waveguide modes

The model in the previous section gives a description of the line shape in the reflectivity of a photonic-crystal slab, but it does not predict the resonance frequencies ω_p. As we will show in this section, it is possible to calculate the resonance frequencies and the waveguide modes for a photonic-crystal slab using a simple model [25,26,32]. In this nearly-free photon approximation, the waveguide is treated as a uniform slab with an effective refractive index that depends on the filling factor of the air holes. For the TE waveguide modes, having the electric field in the plane of the slab, the dispersion relation for a uniform slab is implicitly defined as [14]

$$\sin(hd)\left(h^2 - pq\right) = \cos(hd)(p+q)h, \tag{2.7}$$

where p, q, and h denote the transverse components of the wave vector in the different media. They are defined as $q^2 = \beta^2 - \left(\omega^2/c^2\right) n_0^2$, $h^2 = \left(\omega^2/c^2\right) n_\mathrm{g}^2 - \beta^2$, and $p^2 = \beta^2 - \left(\omega^2/c^2\right) n_\mathrm{s}^2$, where n_0, n_g, and n_s are the refractive indices of the top, guiding, and bottom layer, respectively, and c is the speed of light in vacuo. The condition for coupling to a waveguide mode is given by the diffraction condition

$$\vec{k}_\parallel + \vec{G} = \vec{\beta}, \tag{2.8}$$

where $\vec{k}_\parallel$ is the parallel component of the incident wave vector, $\vec{\beta}$ is the parallel component of the wave vector of the waveguide mode, and $\vec{G}$ is a reciprocal lattice vector of the photonic crystal. For normal incidence, this reduces to

$\vec{\beta} = \vec{G}$, which can be used to numerically find the resonance frequencies ω_m from Eq. (2.7).

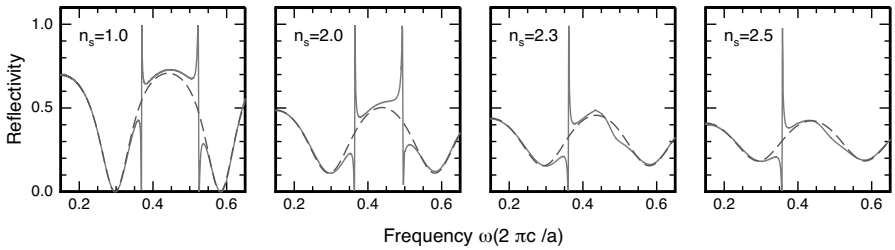

Figure 2.4. Reflectivity of a 1-D photonic-crystal slab, calculated using a FDTD method. The grating consists of air slits with $w/a = 0.1$ in a dielectric slab with $d/a = 0.5$ and refractive index $n_\mathrm{g} = 3.5$, on top of a substrate with increasing refractive index. Two resonances are visible, on top of an oscillating background. The dashed curve is a fit to the background of a refractive index of the form described in Eq. (2.9). The resonance around $\omega = 0.5$ disappears for $n_\mathrm{s} > 2.0$.

For simplicity, we calculated the reflectivity of an one-dimensional (1-D) array of slits, using a freely available FDTD package [33]. The cross section of the structure used in these calculations is given in Fig. 2.3(b). The slab of thickness d and refractive index $n_\mathrm{g} = 3.5$ contains an array of slits of width w and refractive index $n_0 = 1$. The array has a lattice constant a and we used $w/a = 0.1$ and $d/a = 0.5$. The substrate index n_s was varied between 1 and 3.0, and the reflection spectra were calculated at normal incidence for TE-polarized light (E-field parallel to the slits).

Figure 2.4 shows the reflectivity of the array as a function of frequency, for increasing substrate index n_s. Two distinct resonances are visible on top of an oscillating background. The Fresnel reflection coefficient for the layered system can be fitted to the spectra, using an effective refractive index of the form [24]

$$n_\mathrm{g} = c_0 + c_1\omega + c_2\omega^2, \tag{2.9}$$

with c_0, c_1, and c_2 as only fit parameters. Typical values for the fit parameters are $c_0 = 3.25$, $c_1 = 0.42$, and $c_2 = -0.21$, yielding an effective index between 3.25 and 3.46. The result of the fit is shown as the blue dashed lines in Fig. 2.4. The effective index is close to the volume average of the dielectric constants [34, 35] for $\omega < 0.5$, but deviates for higher frequencies. This is due to the fact that for higher frequencies the wavelength becomes comparable to the lattice spacing and slit width, and simple effective-medium theory breaks down.

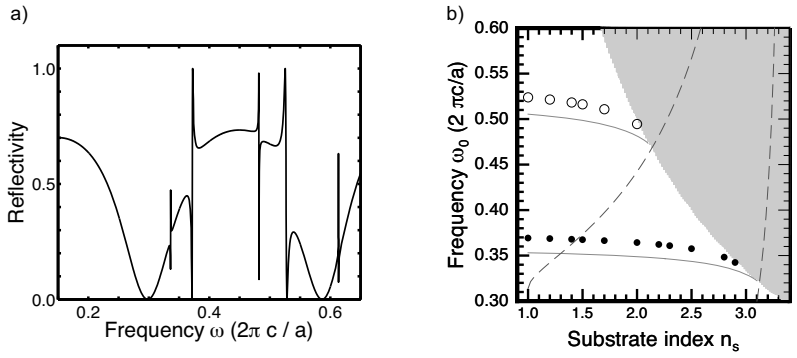

Figure 2.5. (a) Calculated reflectivity of the array of slits at 5° angle of incidence, for a substrate index $n_s = 1$. Two resonances that are not visible at normal incidence appear at $\omega \approx 0.33$ and $\omega \approx 0.48$. (b) Resonance frequencies of the Fano resonances as a function of the substrate refractive index n_s. The resonance frequencies can be predicted using a simple waveguide model (red curves), with n_g given by effective medium theory. This model does not include the avoided crossing between the two waveguide modes, and therefore calculates the average of the high-frequency and low-frequency resonances. The dashed curves correspond to the cut-off conditions of the $m = 0$ and $m = 1$ modes. The gray area indicates the parameter region where higher order diffraction into the substrate occurs.

At normal incidence, the resonances corresponding to a specific reciprocal wave vector $\vec{G}$ are degenerate. Due to the grating, they are coupled and show an avoided crossing. A simple explanation of the fact that we only observe one of the resonances is given in terms of coupled mode theory [36]. For a sinusoidal 1-D grating with a dielectric function that contains only a Fourier component $\epsilon(\vec{G})$, no avoided crossing occurs at normal incidence. The interaction that creates the avoided crossing is caused by the higher harmonics of the dielectric function $\epsilon(\vec{r})$. The coupling to these modes is determined by the relative phase of the Fourier components. For a 1-D square profile, the first and second harmonic are out of phase ($\phi = \pi/2$ in the notation of Ref. 36). The Bloch wave that mediates the coupling to the resonance only has nonzero overlap with the high-frequency mode. This leads to zero coupling strength to the low-frequency mode, and as a consequence, the peaks in Fig. 2.4 are exclusively due to coupling to the high-frequency mode [26]. The fact that we only observe the high-frequency mode at normal incidence is confirmed by the calculation in Fig. 2.5(a), that shows a reflection spectrum for the 1-D grating with a substrate index $n_s = 1$, at an angle of incidence of 5°, calculated using

a rigorous coupled wave analysis [37]. In this figure, the lower-frequency resonances can be seen to appear as narrow resonances at $\omega = 0.33$ and $\omega = 0.48$.

As can be seen in Fig. 2.4, the two resonances visible for $n_s \leq 2.0$ at normal incidence have opposite symmetry. This is consistent with the fact that these resonances are due to the first and second TE waveguide mode, that have an even and odd field distribution, respectively. For a refractive index $n_s > 2.0$, the second resonance is seen to disappear from the spectrum. We fitted Eq. (2.6) to the calculated spectra, using the refractive index obtained by the fit of the oscillating background as an input. The only fit parameters are the resonance frequencies ω_0 and ω_1, and the line widths γ_0 and γ_1. The resulting resonance frequencies are shown as the symbols in Fig. 2.5(b), plotted as a function of the substrate refractive index, and are compared to the numerical solution of Eq. (2.7) (solid curves) obtained using $n_g = 3.34$. The calculated frequencies are below the frequencies obtained from the fits, because the waveguide model predicts the center frequency and does not take into account the avoided crossing. In fact, the data in Fig. 2.5(a) for 5° angle of incidence show that the waveguide model correctly predicts this center frequency.

The disappearance of the resonance is also predicted by the waveguide model. The cut-off frequency of the m-th mode is given by [14]

$$\omega_{cm} = \frac{c}{2\pi d\sqrt{n_g^2 - n_s^2}} \left(m\pi + \arctan \sqrt{\frac{n_s^2 - n_0^2}{n_g^2 - n_s^2}} \right). \tag{2.10}$$

This condition is drawn with dashed curves in Fig. 2.5(b) for the first two waveguide modes, calculated using an effective refractive index $n_g = 3.34$. Diffraction into the substrate occurs at a frequency ω_d, where the propagation constant β becomes equal to the length of the wave vector in the substrate. This leads to the condition

$$\omega_d = (k_{\|} + G)/n_s. \tag{2.11}$$

The existence of diffraction orders at normal incidence is indicated by the grey area in Fig. 2.5(b). This corresponds to the situation where the transverse component of the wave vector in the substrate $p = 0$. The resonance frequency of the waveguide mode *at cut-off* is thus given by the intersection of Eq. (2.10) and Eq. (2.11).

It is important to mention here that although assigning the different resonances to different modes is quite straightforward in the 1-D case, in the 2-D case TE-TM mixing will occur [38]. The mixing between different modes induces avoided crossings between otherwise orthogonal modes, and causes TE

modes to appear in the TM spectra, and vice-versa. This makes identification of specific peaks with specific waveguide modes more complicated.

2.4 Reflection measurements

We measured the specular reflection from the GaAs photonic-crystal slab shown in Fig. 2.1(a) along the Γ-X direction (indicated with the arrow) as a function of the angle of incidence from 25° to 80°. White light from a spectrally broad lamp was polarized and focused onto the sample. The specular reflection was polarization-filtered, imaged onto a fiber, and analyzed in a spectrometer with a spectral resolution of ~ 2 nm. The numerical aperture (NA) of the incoming beam was limited to NA < 0.04. The spot size on the sample was ~ 100 μm.

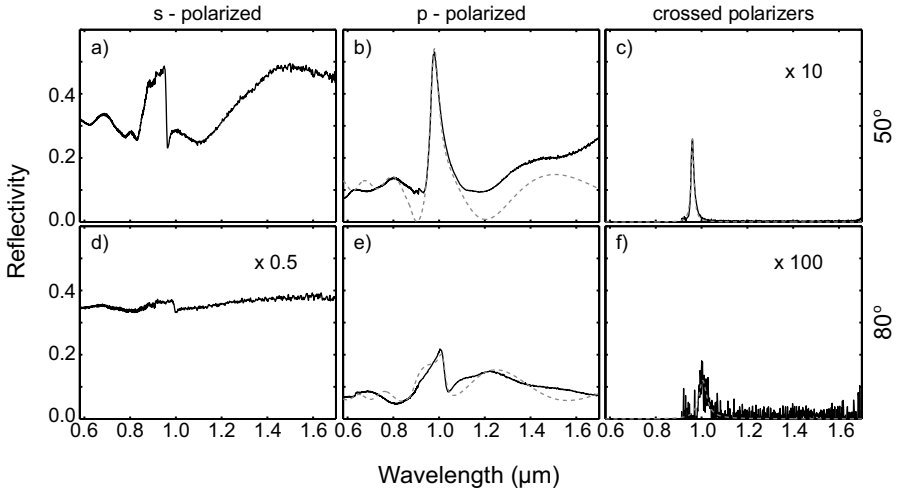

Figure 2.6. Experimental reflection spectra of a photonic-crystal slab for two angles of incidence, 50° [(a) to (c)] and 80° [(d) to (f)], for *s*-polarized [(a) and (d)] and *p*-polarized light [(b) and (e)], and for a crossed polarizer setup, where the incoming light was *p*-polarized and the detected light was *s*-polarized [(c) and (f)]. The dashed curves are fits using the model discussed in the text. Figures (c), (d), and (f) are scaled with the factors indicated, to enhance visibility.

Reflection spectra for angles of incidence of 50° and 80° are shown in Fig. 2.6 for three different settings of the polarizers. Figures 2.6(a) and (d) show the spectra for the situation where both polarizers were set to a polarization perpendicular to the scattering plane (*s*-polarization). An asymmetric

peak around a wavelength of ~ 950 nm is seen on top of an oscillating background. The peak position changes with angle of incidence. Similar peaks can be seen in Fig. 2.6(b) and (e), where both polarizers were set to a polarization parallel to the scattering plane (p-polarization). In this case, the asymmetry of the peak is changed when tuning the angle of incidence from 50° to 80° The symmetry of the peak is the same for both polarizations at 80° angle of incidence.

The Fano model described in Sec. 2.3.1 can be used to describe the observations. We use Maxwell-Garnett's effective medium theory [34,35] to describe the photonic crystal layer as a homogeneous birefringent layer with an effective refractive index n_{eff}, incorporating the known refractive index dispersion of GaAs [39]. This includes absorption for wavelengths shorter than 950 nm. With this effective index, we calculate the polarization- and angle-dependent Fresnel reflection and transmission coefficients of the layered system.

The dashed curves in Fig. 2.6 show fits of the Fano model to the measurements. The only fit parameters were the resonance frequency ω_0, the linewidth γ, and the waveguide losses Γ. We slightly adjusted the effective index n_{eff} for different angles of incidence, to get a better fit to the oscillating background. Although the fits deviate on detail from the measurements, qualitatively all elements of the measurement are contained in the model. We attribute most deviations to the simplifications we made with respect to the vertical shape of the air holes, and to the fact that effective medium theories only hold when all relevant length scales in the system are much smaller than the wavelength. In fact, the tapering of the holes is essential to observe the resonances. It ensures that there is a waveguiding layer in the top part of the photonic-crystal structure, that provides a discrete mode.

The Fano model also gives a direct explanation for the change in asymmetry of the peak. Since the peak shape is determined by interference of a resonant and a direct channel, the relative phase between these two contributions determines the asymmetry of the resulting peak. The Fresnel coefficient r for s-polarized light is always negative, but the Fresnel coefficient for p-polarized light vanishes and changes sign at Brewster's angle. It is exactly this change of sign that causes the line shape to change when the angle of incidence is tuned to larger angles (see Ch. 3 and Refs. 40,41). The fact that the asymmetry for s-polarized light is the same as for p-polarized light at large angles of incidence indicates that both peaks are due to coupling to a waveguide mode that is even in the center plane of the photonic-crystal slab.

In Fig. 2.6(c) and (f) the reflection spectra of the photonic-crystal slab is shown in a setup where the incoming light was p-polarized, and the collected

light was s-polarized. A small Lorentzian-shaped peak can be observed in these spectra. The resonance frequencies obtained from the fits of the different measurements are not exactly identical for the same angle of incidence. This indicates that the peaks in Fig. 2.6(a), (b), and (c) are due to different waveguide modes. Since Fresnel reflection is polarization-maintaining for s- and p-polarization, the direct channel is filtered out by the second polarizer. This results in a resonant contribution only, explaining the Lorentzian line shape of the peak [42]. The intensity of these peaks is low, because the symmetry of the photonic-crystal lattice dictates that the polarization (s or p) is conserved upon transmission and reflection, as long as the wave vector $k_{\|}$ is along one of the symmetry directions of the lattice. The fact that we do observe a small peak demonstrates that our structure does not have perfect square symmetry.

2.5 Conclusion

In summary, the typical asymmetric peaks on top of an oscillating background, observed in the reflection from a photonic-crystal slab, are due to interference between a direct and a resonant reflection channel. The observed change of asymmetry of the peak, for p-polarized light, is caused by a change of sign of the direct reflection at Brewster's angle. This asymmetry change will be discussed in detail in Ch. 3. The rough shape of the holes in our experiment causes relatively broad spectral features that are easily resolved. The fact that we are able to describe our data with a coupled mode theory and observe the change in asymmetry of the spectral line shows that the description is robust and also valid for less-than-perfect photonic crystals.

The frequencies of the resonances can be predicted using a simple waveguide model, using the effective index of the guiding layer as the only adjustable parameter. This model can be used to predict the disappearance of certain resonances from the reflectivity spectrum, when changing the substrate refractive index. The predictions for waveguide cut-off of the second TE mode are confirmed by FDTD calculations of the reflectivity. The ability to control the coupling to specific modes can be an important design parameter for photonic crystal structures, if coupling to a specific mode is undesirable. Another possible application is to create an optical switch, where a change in the optical parameters of the guiding layer can be used to temporarily transform one of the guided modes into a leaky mode.